Detailed Boundary Layer Measurements on a Turbine Stator Vane at Elevated Freestream Turbulence Levels

R. W. Radomsky[1]
e-mail: roger_w_radomsky@raytheon.com

K. A. Thole
e-mail: thole@vt.edu

Mechanical Engineering Department,
Virginia Polytechnic Institute
and State University,
Blacksburg, VA 24060

High freestream turbulence levels have been shown to greatly augment the heat transfer on a gas turbine airfoil. To better understand these effects, this study has examined the effects elevated freestream turbulence levels have on the boundary layer development along a stator vane airfoil. Low freestream turbulence measurements (0.6 percent) were performed as a baseline for comparison to measurements at combustor simulated turbulence levels (19.5 percent). A two-component LDV system was used for detailed boundary layer measurements of both the mean and fluctuating velocities on the pressure and suction surfaces. Although the mean velocity profiles appeared to be more consistent with laminar profiles, large velocity fluctuations were measured in the boundary layer along the pressure side at the high freestream turbulence conditions. Along the suction side, transition occurred further upstream due to freestream turbulence.
[DOI: 10.1115/1.1424891]

Introduction

Accurate predictions of surface heat loads on an airfoil are made difficult by the complex flow structure surrounding the airfoil. Boundary layers developing on a vane or blade surface are subjected to a combination of variables including freestream turbulence, surface curvature, roughness, favorable and unfavorable pressure gradients, boundary layer transition, relaminarization, and stagnation point flow. Numerous investigations have been performed in the past that have addressed the isolated effects of most of these variables on boundary layer development with the majority of the studies being performed on simple flat plate or cylinders-in-crossflow geometries. To incorporate all of the variables affecting boundary layer development on gas turbine airfoils, studies need to be performed on geometries representative of those found along an airfoil. While there have been a few studies performing boundary layer measurements on an airfoil surface, these studies have been made at relatively low freestream turbulence conditions. To date, no studies have been performed on a turbine airfoil geometry at turbulence levels representative of those exiting current gas turbine combustors.

Turbulence measurements taken at the exit of a variety of gas turbine combustors have shown that the levels can range between 8 percent and 40 percent (Goldstein et al. [1]; Kuotmos and McGuirk [2]; and Goebel et al. [3]) with an indication that the integral length scale is dictated by the diameter of the dilution holes in the combustor (Moss [4]). Although the turbulent kinetic energy levels actually increase through the downstream airfoil passage due to the velocity gradients experienced by the flow (Radomsky and Thole [5]), the local turbulence levels, particularly along the suction side, decrease as the flow is accelerated. The effect that these high turbulence levels has on the airfoil is to significantly increase the heat transfer along the leading edge and pressure side surfaces as well as move the transition location forward on the suction side surface. Typically, the increase in turbulent kinetic energy in the passage is not accounted for in the current boundary layer codes, which assume decay rates similar to that occurring downstream of a grid. Thus, it is important to generate an experimental database to use as a benchmark for improving predictive tools for the purpose of more accurately capturing the physics of the flowfield.

Past Studies

As stated previously, most of the boundary layer studies examining various flowfield effects have used a flat plate geometry. These studies, which started as early as Kestin [6], are far too numerous to completely discuss in this paper. A few of the more relevant investigations in which boundary layer measurements have been made along an airfoil will be discussed in the following paragraphs.

Detailed boundary layer measurements have been made on an airfoil surface by Ubaldi et al. [7], Bario and Beral [8], and Lee and Kang [9]. Ubaldi et al. [7] performed detailed boundary layer measurements at low freestream turbulence conditions in a large-scale turbine vane cascade at low turbulence levels. The measurement technique that they used was a two-component LDV system with a probe volume size that ranged between a $10<D^+<40$. Ubaldi et al. [7] reported that the boundary layers on the pressure side of the vane remained ''laminar in shape'' along the majority of the pressure surface although large streamwise fluctuations were present inside the boundary layer.

Measurements reported by Bario and Beral [8] were for a scaled up stator vane geometry in which they used a two component LDV system. The freestream conditions included two turbulence levels at Tu=0.6 and 5 percent. For the turbulent profiles, the increased turbulence penetrated into the boundary layer causing elevated levels of streamwise fluctuations in the transition region. An increase in the correlation coefficient was also observed in the boundary layer for the higher turbulence levels, which was the opposite trend to that observed by Thole and Bogard [10] for flat plate boundary layers. They attributed these increases to the highly correlated turbulence outside of the boundary layer.

Lee and Kang [9] compared low freestream turbulence conditions to levels as high as 15 percent that they were able to simulate by placing their symmetric airfoil in the downstream wake of another airfoil. Note that the wake flowfield is fundamentally

[1]Presently at Raytheon, Tuscon, AZ 85734.

Contributed by the International Gas Turbine Institute and presented at the 46th International Gas Turbine and Aeroengine Congress and Exhibition, New Orleans, Louisiana, June 4–7, 2001. Manuscript received by the International Gas Turbine Institute February 2001. Paper No. 2001-GT-169. Review Chair: R. Natole.

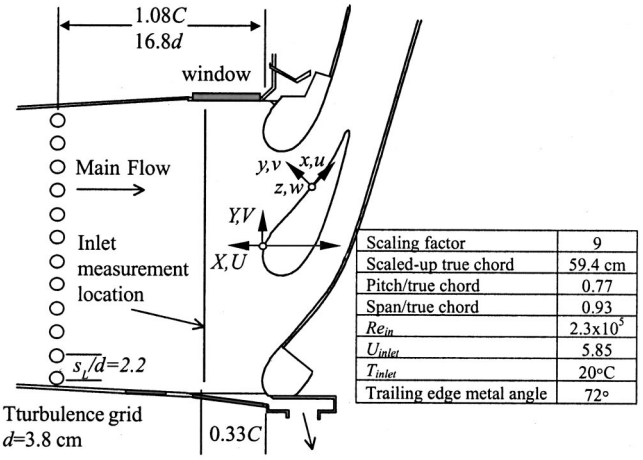

Scaling factor	9
Scaled-up true chord	59.4 cm
Pitch/true chord	0.77
Span/true chord	0.93
Re_{in}	2.3×10^5
U_{inlet}	5.85
T_{inlet}	20°C
Trailing edge metal angle	72°

Fig. 1 Schematic of stator vane test section

different from the one studied in our paper for the following two reasons: i) there exists a mean velocity deficit from the upstream airfoil wake that impacts the airfoil leading edge, and ii) the turbulence level outside of the wake region is low. At low freestream turbulence conditions, the measured streamwise velocity fluctuations near the wall appeared to go from a two-peaked profile to a single peaked profile as the mean velocity profiles transitioned from laminarlike to fully turbulent. At high freestream turbulence conditions, their results indicated the presence of high streamwise velocity fluctuations even though the mean profile appeared laminar in shape for the case with high freestream turbulence conditions.

Although these studies have given an indication of boundary layer development on an airfoil surface, there is a need for detailed measurements at turbulence levels representative of those exiting typical gas turbine combustors. This paper represents one in a series of papers that have documented highly turbulent flow through a first-stage vane passage. Midspan turbulence measurements and surface heat transfer measurements were reported by Radomsky and Thole [5] while the effects of freestream turbulence in the endwall region were reported by Radomsky and Thole [11]. These previous two papers in addition to the present paper provide a complete database for computational benchmarking.

Experimental Design

The details of the recirculating wind tunnel and design of the stator vane test section used in this study have been documented thoroughly in a number of previous studies including Kang et al. [12], Kang and Thole [13] and Radomsky and Thole [5,11,14]. A schematic of the stator vane test section and a table showing the relevant geometrical parameters and operating conditions are given in Fig. 1. Note that the metal angle is the average angle of the pressure and suction sides, which is 72 deg for our case, while the flow angle is the angle at which the flow leaves the passage relative to the inlet, which is 78 deg for our case. To allow for highly resolved boundary layer measurements, the vane cascade was geometrically scaled-up by a factor of nine. The inlet Reynolds number to the test section was matched to that of an engine; however, the inlet Mach number could not be matched due to the increased scale of the test section. It can be shown using the boundary layer equations that if the acceleration parameter and momentum thickness Reynolds numbers are matched, the flow field between the compressible and incompressible conditions will also be matched (Polanka [15]).

The test section consisted of an instrumented central vane in addition to the leading edges of two adjacent vanes. A flexible plexiglass sidewall, which allowed optical axis for LDV measurements, was attached to the leading edges of the vane. The flexible wall was placed to exactly match the geometry of an adjacent vane. Downstream of where the adjacent airfoil would end, the location of the flexible wall was placed to match the pressure distribution predicted by a two-dimensional, low-speed, inviscid calculation. Static pressure measurements on the vane were performed to insure the correct placement of the flexible wall in addition to insuring periodic flow was achieved between the two passages.

Heat transfer measurements were made on the polystyrene central vane, which was wrapped with five 50-micron-thick type 304 stainless steel foils. The metal foils provided a constant heat flux boundary condition. Beneath the stainless steel foil and embedded in the styrofoam 58 type E thermocouples were placed. The spanwise position for the thermocouples was at 40 percent of the span measured from the bottom endwall.

A few changes were implemented to the experimental setup that differed from the descriptions given in the aforementioned investigations. In order to accurately measure boundary layers with a laser Doppler velocimetry (LDV) system, which was the main objective of the investigation, a surface must be both smooth and nonreflective. For this reason, a new instrumented central vane was constructed to replace the original vane which had the metallic constant heat flux surface. As with the original vane, the new vane was also constructed from stacking pieces of 2-in. rigid Styrofoam insulation that was cut to shape using a template and an electrically heated wire. The Styrofoam cutouts were epoxied together to achieve the necessary span/chord ratio given in Fig. 1. The entire vane was sanded to achieve the correct profile and eliminate any steps between adjacent cutouts. Upon achieving a smooth surface, the entire vane was then covered with several layers of fiberglass. After the final layer of fiberglass was applied, the vane was sanded and painted repeatedly using progressively finer sand paper until a smooth, flat black surface was achieved. A description of the process is found in Radomsky [16].

The second change in the experimental setup involved the method for generating elevated freestream turbulence levels. Due to a change in the location of the experimental facility, the compressed air system required for the active-grid turbulence generator was no longer available. As a result, a different technique for generating turbulence levels of 20 percent was required. Previous work at the University of Texas showed that turbulence levels of 20 percent and length-scale-to-pitch ratios of $\Lambda_x/P=0.091$ could be obtained using a passive grid system (Polanka, [15]). Note that these are the same level and scale of the turbulence used in Radomsky and Thole [5,11]. The passive grid design consisted of a series of 3.8-cm-dia bars with a lateral spacing of $s_L/d=2.2$. The bar size and the close spacing between the bars was reported to eliminate the shedding from the bars in the region where measurements were performed. As will be shown later, good agreement in the turbulence level was achieved between the two turbulence generator techniques.

Methods Used for Boundary Layer Measurements

Boundary layers at nine streamwise locations were measured with the LDV system on the vane at the midspan location. The location of boundary layer measurements on the vane surface can be seen in Fig. 2. Boundary layer profiles were measured at four streamwise locations on the pressure surface. These locations correspond to streamwise distances of $s/C=-0.15$ (P1), -0.30 (P2), -0.45 (P3), and -0.60 (P4) from the vane stagnation location. Boundary layer profiles were measured at five streamwise locations on the suction surface corresponding to streamwise distances of $s/C=0.21$ (S1), 0.50 (S2), 0.75 (S3), 1.00 (S4), and 1.25 (S5). The boundary layer measurements used a local coordinate system, as shown in Fig. 1, where the origin was located at the vane surface at the desired streamwise location. One axis of the coordinate system was aligned parallel (x), while the other axis was

Name	Location	D^+
SP	$s/C=0$	stagnation
Pressure Side		
P1	-0.15	0.9
P2	-0.3	1.3
P3	-0.45	1.6
P4	-0.60	1.8
Suction Side		
S1	0.21	2.7
S2	0.5	3.1
S3	0.75	1.2
S4	1.0	1.3
S5	1.2	3.4

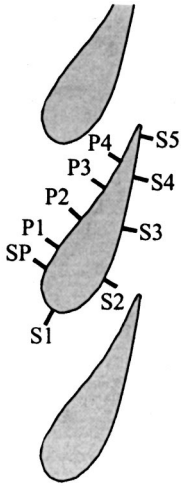

Fig. 2 Location of boundary layer measurements

normal (y) to the surface. To completely document the boundary layer structure, a minimum of 20 measurement locations were measured in each of the boundary layer profiles.

A two-component back-scatter fiber optic LDV system used in this study consisted of a 5 W laser and a TSI model 9201 Colorburst beam separator. Velocity data was processed using TSI model IFA 755 Digital Burst Correlator controlled using TSI's FIND software. To keep the measurement volume as small as possible, a beam expander and 450 mm focusing lens were used. This resulted in a probe diameter, which is the coordinate normal to the surface, of 44 μm and a probe volume length of 0.32 mm. In addition to the location of the measurements, Fig. 2 also shows the nondimensional diameter of the probe volume (D^+), in terms of inner wall coordinates, at each of the measurement locations. The LDV probe was tilted at the half-angle of the beams, $\kappa = 7.78$ deg, to allow for measurements very near the vane surface. For the noncoincident LDV measurements, each mean and rms velocity were averaged over 12,000 points, which took nominally 20 s to acquire. For coincident LDV measurements, using a coincidence window of 10 μs, each mean and rms velocity were averaged over 25,000 points to allow for accurate determination of higher order velocity statistics. All measurements were corrected for bias errors using the well-accepted time weighted average correction scheme.

The location of the wall during boundary layer measurements was estimated using two techniques. The first technique involved lowering the input power to the LDV system and visually monitoring the crossing of the beams on the vane surface. The second technique was to monitor the output from the photomultiplier tubes using an oscilloscope. Both methods for locating the wall produced nearly identical results. From numerous repeatability studies, it was determined that the location of the wall was known to within ± 20 μm. For the present investigation, this value corresponds to a distance from the wall in wall coordinates of at most a $y^+=2$ at a $s/C=1.2$.

Boundary layer measurements will be presented in terms of both freestream variables and inner variables. When presenting the data in terms of inner variables, knowledge of the shear velocity, $u_\tau = \sqrt{\tau_w/\rho}$, is required. For laminar, flat plate boundary layer flows, the shear velocity is typically determined by calculating the velocity gradient near the wall where the profile is linear. For a laminar boundary layer affected by a strong pressure gradient there is additional stress added by the pressure gradient, $\tau_w = \mu(du/dy) - y(dP/ds)$ (Kays and Crawford [17]). This relation, however, does not consider any momentum flux term. In analyzing the measured velocities close to the wall, we determined that the mean velocities indicated a linear relation with distance from the wall. This implies that the pressure gradient term is not affecting the velocities in the near wall region and that the additional pressure force is balanced by the momentum flux difference. For that reason, the wall shear stress used in the data presented in this paper was that calculated from the slope of the velocity at the wall.

Generally for turbulent boundary layers, the shear velocity is determined using a Clauser fit in the log-law region of the velocity profile. This is because the physical distance to the wall where $u^+=y^+$ is very small making it difficult to measure the viscous sub-layer velocities. The Clauser fit technique has been shown by Thole and Bogard [10] to be a valid method of estimating u_τ even at high freestream turbulence conditions of 20 percent.

The most difficult region for estimating u_τ is where a transitional boundary layer is present. In this region, as with the laminar profiles, measurements were performed in the viscous sublayer to allow the data to be fit to the $u^+=y^+$ relationship. This requires measurements very near the wall surface. For all of the measurements to be discussed, the closest measurement was typically 0.08 to 0.10 mm from the surface of the vane. For laminar boundary layers, this distance typically corresponded to y^+ values of $y^+ \sim 5$. For transitional and turbulent boundary layers the closest measurement location was a $y^+ \sim 8$ to 10.

Uncertainty Estimates

The partial derivative and sequential perturbation methods, described by Moffat [18], were used to estimate the uncertainties of the measured values. Uncertainties were calculated based on a 95 percent confidence interval. The estimate of bias and precision uncertainties for the mean velocities were 1 percent, while the precision of the rms velocities was 1.2 percent for u_{rms} and 1.7 percent for v_{rms}. The precision uncertainties of the Reynolds shear stress and correlation coefficient were 4.8 percent and 5.4 percent. Note that these uncertainty estimates were at the high freestream turbulence conditions near the surface on the suction side of the vane. The total uncertainty in the Stanton numbers was 4 percent at the leading edge and 5 percent at the trailing edge on the suction side of the vane. The total uncertainty in the friction factor was a maximum of 7.5 percent for a laminar boundary layer and 5 percent for a turbulent boundary layer.

Inlet Flow Conditions

Profiles of the mean velocity and turbulence components were measured at one-third chord upstream ($X/C=-0.33$) for inlet turbulence levels of Tu = 19.5 percent. Figure 3(a) shows streamwise and pitchwise mean velocity profiles measured across the entire pitch of two vane passages using the passive-grid and previously reported active grid turbulence generators. These measurements were compared to a baseline case, measured at low freestream turbulence conditions of Tu = 0.6 percent, and to a CFD prediction using the Reynolds stress turbulence model (RSM) at freestream turbulence levels of Tu = 1 percent (Radomsky and Thole [5]). The mean velocities have been normalized by the inlet approach velocity, U_{inlet}. A global coordinate system, as shown in Figure 1 with the origin at the stagnation point of the center vane ($Y/P=0$), was maintained for the results shown in Fig. 3(a). At this upstream location, the mean velocity was just beginning to feel the effects of the stator vane, as is evident by the deceleration in U/U_{inlet} observed in front of the central vane ($Y/P=0$). As the streamlines turn around the vane, slightly positive pitchwise velocities (V/U_{inlet}) occurred near the stagnation point for $Y/P>0$ and slightly negative pitchwise velocities occurred near the stagnation for $Y/P<0$. Although the turbulence levels were very high, the good agreement with the low freestream turbulence case and CFD prediction shows the mean flowfield was unaffected by either of the turbulence generators.

Turbulence levels and length scales were measured across the entire pitch of the two passages at $X/C=-0.33$. Figure 3(b)

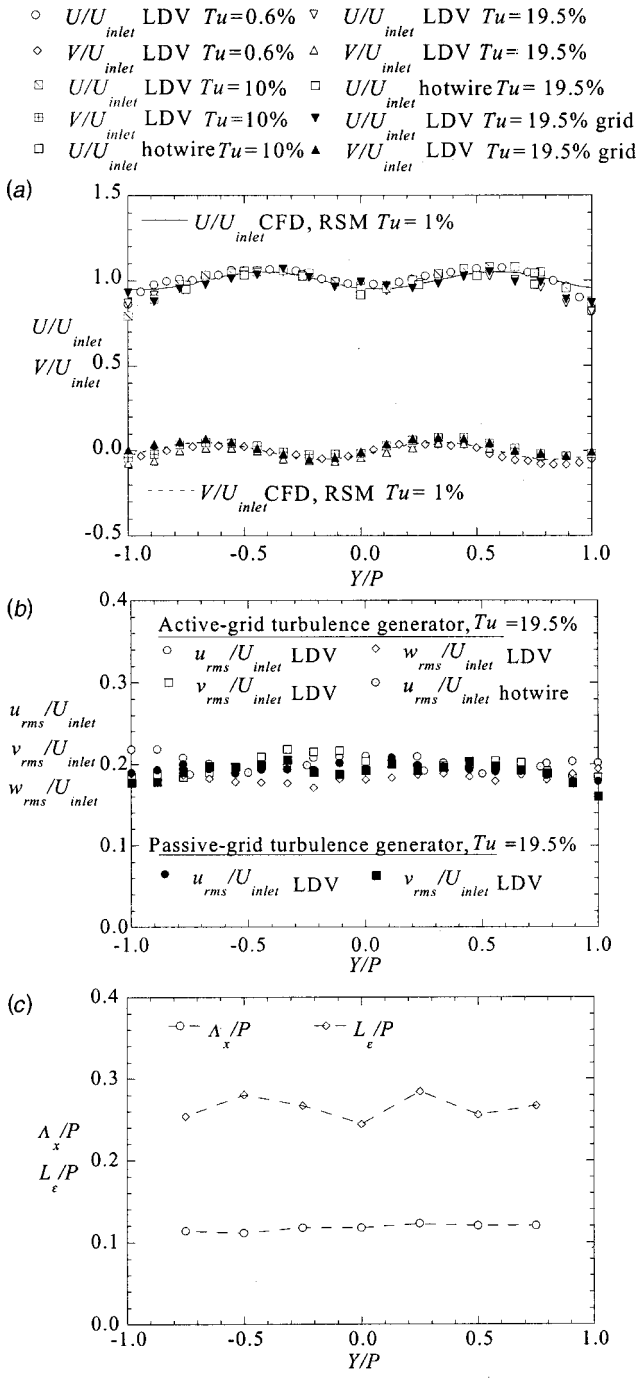

Fig. 3 Profiles of: (*a*) normalized streamwise, U/U_{inlet}, and pitchwise, V/U_{inlet}, velocities at various turbulence levels and measurement techniques, (*b*) streamwise (u_{rms}/U_{inlet}), pitchwise (v_{rms}/U_{inlet}) and spanwise (w_{rms}/U_{inlet}) turbulence levels, and (*c*) integral and dissipation length scales measured at $X/C=-0.33$

shows the streamwise ($u_{\rm rms}/U_{\rm inlet}$), pitchwise ($v_{\rm rms}/U_{\rm inlet}$), and spanwise ($w_{\rm rms}/U_{\rm inlet}$) rms levels at an inlet turbulence level of 19.5 percent using two different turbulence generators. The maximum deviations relative to the average for the streamwise and pitchwise rms levels were 7.8 percent and 7.6 percent for the 19.5-percent case. No noticeable difference was observed in the level or uniformity of the turbulence between the different turbulence generators. Fig. 3(*c*) shows the measured integral and dissipation length scales across the passages with the integral scale being approximately 11 percent of the pitch.

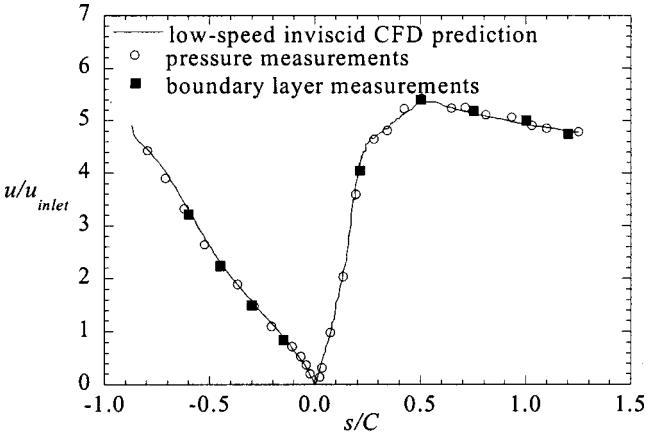

Fig. 4 Comparison of inviscid velocity distribution from static pressure and LDV boundary layer measurements to the low-speed inviscid CFD prediction

As a check for the boundary layer measurements, a comparison was made between measured edge velocities, the calculated velocities from the measured static pressure distribution, and the predicted velocities from an inviscid CFD simulation. Figure 4 shows this comparison and indicates good agreement between the two independent measurements. The positive values of s/C refer to the suction surface, while the negative values indicate the pressure surface. Figure 4 also illustrates the inviscid velocities affecting the boundary layer development. On the pressure side there is a constant acceleration, with an acceleration factor of $K=3.14\times10^{-6}$ over the majority of the surface, as the flow progresses from the stagnation to the end of the vane. The inviscid velocities along the suction side show a much different behavior with a rapid acceleration up to $s/C=0.2$ with very high acceleration parameters between $1.1\times10^{-6}<K<0.01$. From $s/C=0.2$ to 0.5, there is a continual acceleration but at a much lower rate having an average acceleration of $K=1.1\times10^{-6}$. Beyond $s/C=0.5$, there is a slight adverse pressure gradient giving a $K=-1.6\times10^{-8}$.

For computational benchmarking purposes, the tables shown in Appendix A1 and A2 of this paper indicate the local boundary layer edge velocities, local edge turbulence levels, and boundary layer parameters for each of the measurement locations. As can be seen by these levels, the local turbulence levels along the suction side decreased rapidly as the flow accelerates while the levels along the pressure side remained slightly higher.

Boundary Layer Parameters

In this section, comparisons will be made of the boundary layer parameters at low and high freestream turbulence levels. These parameters include the boundary layer and momentum thicknesses, the shape factor, friction coefficients, and Stanton numbers. When possible the values will be compared to correlation results using the Thwaites [19] method. The Thwaites method provides a correlation for laminar boundary layers when affected by a pressure gradient.

Figure 5(*a*) compares the measured boundary layer thickness, δ/C, at turbulence levels of 0.6 percent and 19.5 percent to the Thwaites prediction. On the pressure surface, for the 0.6 percent turbulence level, the constant flow acceleration resulted in nearly a constant boundary layer thickness. In contrast, the elevated turbulence level had a large impact on the size of the boundary layer on the pressure surface. At the trailing edge of the pressure surface, the boundary layer thicknesses at the 19.5-percent condition are nearly double those at the 0.6 percent level. On the suction surface, at both turbulence levels, the boundary layer thickness initially decreased in size to a minimum at an $s/C=0.21$ due to the large acceleration at this location. Downstream of location

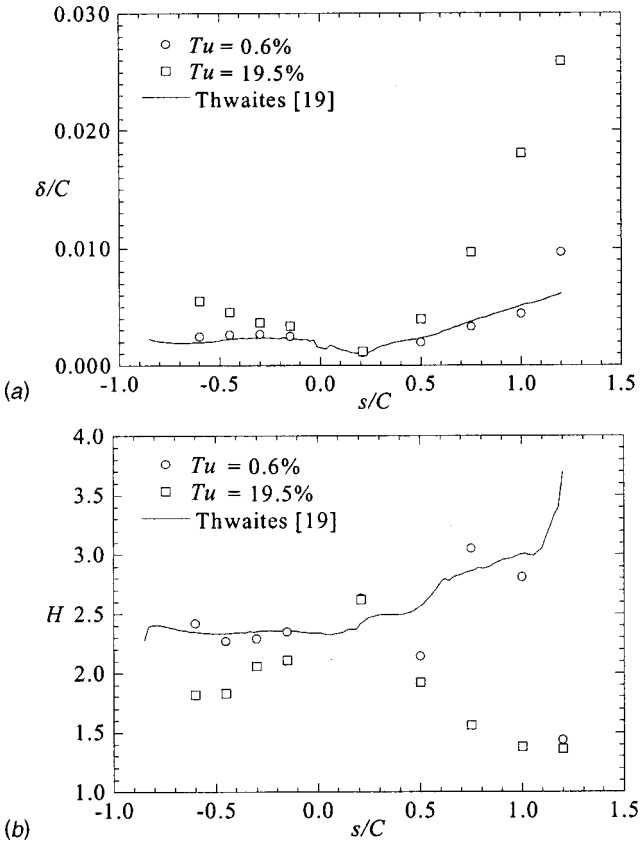

Fig. 5 Comparison of measured: (*a*) boundary layer thickness, δ/C, and (*b*) shape factor, *H*, at turbulence levels of 0.6 percent and 19.5 percent with predictions given by Thwaites [19]

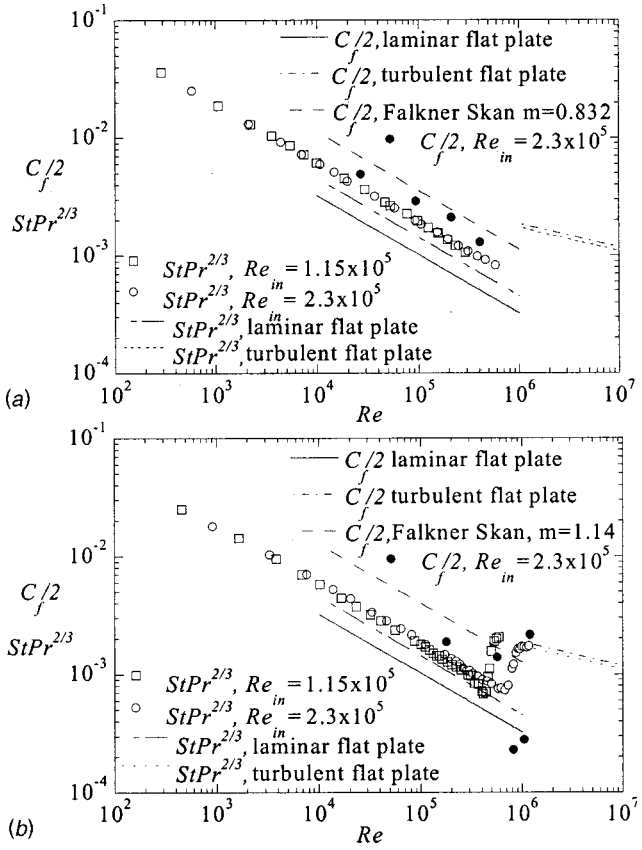

Fig. 6 Comparison of measured Stanton number and friction coefficients on: (*a*) the pressure surface, and (*b*) the suction surface at Tu=0.6 percent

$s/C=0.5$, in the adverse pressure gradient region, the thickness increased quickly. At the high freestream turbulence conditions, there was a sharp rise in the thickness of the suction side boundary layers due to earlier transition to a turbulent boundary layer. The Thwaites [19] method was able to accurately predict the boundary layer thickness over both surfaces at low turbulence conditions up to the point of transition.

The measured displacement and momentum thicknesses are given in Appendix A1 and A2 of this paper. On the pressure surface at low freestream turbulence the pressure gradient caused nearly a constant momentum thickness. At high turbulence conditions, the momentum thickness increased towards the trailing edge of the pressure surface. On the suction surface at low turbulence conditions, the momentum thickness grew steadily from a minimum that occurred at $s/C=0.21$. At high freestream turbulence conditions, the momentum thickness deviated quickly from the low freestream turbulence values as transition began near an $s/C=0.5$.

The ratio of the displacement thickness to the momentum thickness is defined as the shape factor, $H=\delta^*/\theta$. The shape factor for a laminar boundary layer along a flat plate is 2.6. In general, for a laminar boundary layer, favorable pressure gradients tend to steepen the mean velocity profile thereby decreasing the shape factor and adverse pressure gradients flatten the mean velocity profiles thereby increasing the shape factor (Schetz [20]). Figure 5(*b*) compares the measured and predicted shape factor for the 0.6 percent and 19.5 percent conditions. On the pressure surface at low freestream turbulence, the shape factor was essentially constant at a value near 2.4. On the suction surface, at low freestream turbulence levels, the shape factor was near 2.6 at an $s/C=0.21$. At location S2 ($s/C=0.5$), the shape factor decreased to 2.1 indicating that transition was beginning. Downstream at an $s/C=0.5$, the shape factor has decreased due to the favorable pressure gradient occurring up to this point. Farther downstream, the shape factor increased to a value near 3 due to the presence of the adverse pressure gradient. After transition the shape factor decreased to 1.4, which is typical of a turbulent boundary layer. At the elevated turbulence levels, the shape factor on the pressure surface decreased below 2. On the suction surface at elevated turbulence levels, the shape factor quickly fell below 2 at location S2 and reached the fully turbulent values of 1.4 at location S4.

The friction coefficient and the Stanton number distribution at the low turbulence level are plotted for the pressure surface as a function of surface Reynolds numbers in Fig. 6(*a*). Note that the local edge velocities are used as the velocity scales in Re, C_f, and St. The surface distance from the stagnation location is used in Re. In addition to the friction coefficient measurements, heat transfer data measured at identical operating conditions are also shown. Stanton numbers are given at two inlet Reynolds numbers of $\mathrm{Re_{in}}=1.15\times10^5$ and 2.3×10^5 at turbulence levels of 0.6 percent. The Stanton number curves for the two Reynolds numbers fall on the same curve for the pressure surface. Both the friction coefficient and heat transfer data indicate the boundary layer remained laminar over the entire surface.

Both data sets fell above their respective correlations for laminar boundary layer flow over a flat plate. The increased friction and heat transfer is a result of the presence of a favorable pressure gradient caused by the flow accelerating in the vane passage. These data were also compared with a prediction using the Falkner-Skan similarity approach for a laminar boundary layer, which accounts for the streamwise pressure gradients. The friction coefficients fell below the Falkner-Skan prediction, but the agreement was better than observed with the flat plate correlations.

The friction coefficient and the Stanton number distribution at

low turbulence level are plotted for the suction surface as a function of surface Reynolds numbers in Fig. 6(*b*). Both the friction coefficient and heat transfer data initially indicated a laminar boundary layer. As with the pressure surface, the data was above the respective flat plate correlations due to the favorable pressure gradient. The flow was accelerated up to the location of the second boundary layer measurement at an $s/C=0.5$ ($\mathrm{Re}=6\times10^5$). The friction coefficient at this location indicates an increase in the slope of the friction coefficient suggesting that transition was beginning at this location. This transition assertion is supported by the velocity measurements, which showed a mean profile that was beginning to appear turbulent (decrease in the boundary layer shape factor) and a turbulence profile that showed some fluctuations. Downstream of this location, the boundary layer was subjected to an adverse pressure gradient and the measured friction coefficient at locations S3 and S4 showed a dramatic decrease in magnitude. The adverse pressure gradient prevented a full transition from occurring. The decrease in the friction coefficient was the result of the adverse pressure gradient affecting the development of the boundary layer in the near wall region as will be shown later by the boundary layer measurements. Similar dramatic decreases in the friction coefficient for laminar boundary layer flows in the presence of an adverse pressure gradient have been observed by Mislevy and Wang [21]. Farther downstream, at a location of $s/C=1.2$ ($\mathrm{Re}=1.2\times10^6$), the measured friction coefficient indicated that transition from a laminar to turbulent boundary layer had been completed.

The Stanton number curve also indicated that transition began near location S2 ($\mathrm{Re}=5\times10^5$) where the friction coefficient initially started to increase. The heat transfer on the vane was not as affected by the adverse pressure gradient and transition proceeded normally. Greater effects on the friction coefficients as compared to the Stanton numbers were observed in transitioning boundary layers subjected to adverse pressure gradients in Mislevy and Wang [21]. The Stanton numbers for the two Reynolds numbers initially fell along the same curve in the favorable pressure gradient region. The presence of the adverse pressure gradient caused transition to occur at both Reynolds numbers near the trailing edge.

Figure 7(*a*) shows the friction coefficients at 19.5 percent and Stanton numbers on the pressure surface at 10-percent and 19.5-percent turbulence levels. Both the friction coefficient and Stanton numbers indicate that over a majority of the surface a laminar boundary layer was present, with magnitudes higher than those at 0.6 percent turbulence levels. At the higher Reynolds number (near the trailing edge), both the friction coefficients and Stanton numbers began to increase slightly, indicating the onset of transition.

Figure 7(*b*) displays the friction coefficient at 19.5 percent and Stanton numbers on the suction surface at 10-percent and 19.5-percent turbulence levels. Comparisons to Fig. 6(*b*) show that transition occurs at a lower Reynolds number near $\mathrm{Re}=4\times10^5$ as compared to $\mathrm{Re}=6\times10^5$ at low freestream turbulence conditions. The dip in the friction coefficient is not observed at high freestream turbulence conditions because the boundary layer transitioned prior to the onset of the adverse pressure gradient. This resulted in an increase in momentum in the near wall region which resulted in less of a decrease in the friction coefficient for the adverse pressure gradient under high freestream turbulence.

Figure 7(*c*) shows the augmentations of the Stanton number and skin friction due to high freestream turbulence. In general, the heat transfer augmentation was greater than the skin friction augmentation. The heat transfer was augmented by as much as 80 percent for the highest turbulence levels on the pressure side. The large spikes on the suction side are due to the upstream shift in the transition location.

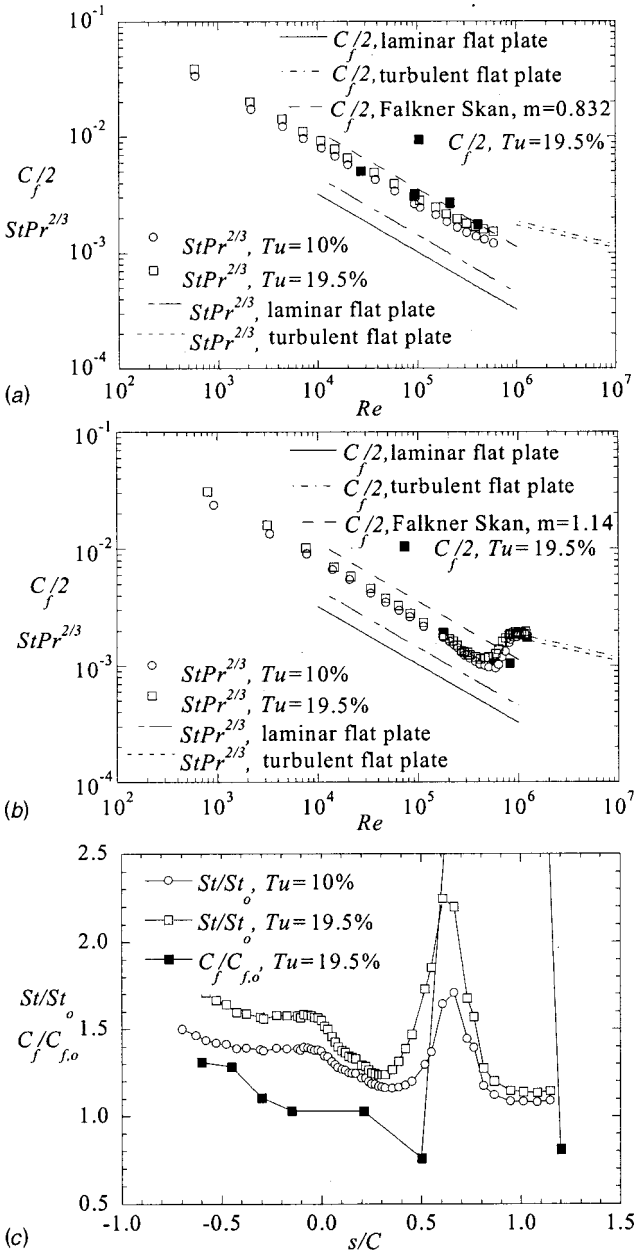

Fig. 7 Comparison of measured Stanton number and friction coefficients on: (*a*) the pressure surface, (*b*) the suction surface at Tu=19.5 percent, and (*c*) friction coefficient, Cf/Cf_o, and Stanton number augmentation, St/St_o, at turbulence levels of 10 percent and 19.5 percent at $\mathrm{Re}=2.3\times10^5$

Boundary Layer at Low Freestream Turbulence

The boundary layer profiles discussed in this section will be presented using two scaling methods. The first method uses outer variables for the normalization scheme. The distance from the surface is normalized by the boundary layer thickness, δ, and the velocity and turbulence statistics are normalized by the inviscid velocity at the edge of the boundary layer, U_{edge}. The second method uses inner wall scaling parameters, which are a function of the shear velocity, u_τ, and viscosity, ν.

Pressure Surface. Figure 8(*a*) shows the mean velocity profiles measured on the pressure surface plotted in terms of freestream parameters. Predictions at $s/C=-0.15$ and $s/C=-0.60$ using the method given by Pohlhausen [22] for laminar boundary layers are also given in Fig. 8(*a*). This boundary layer

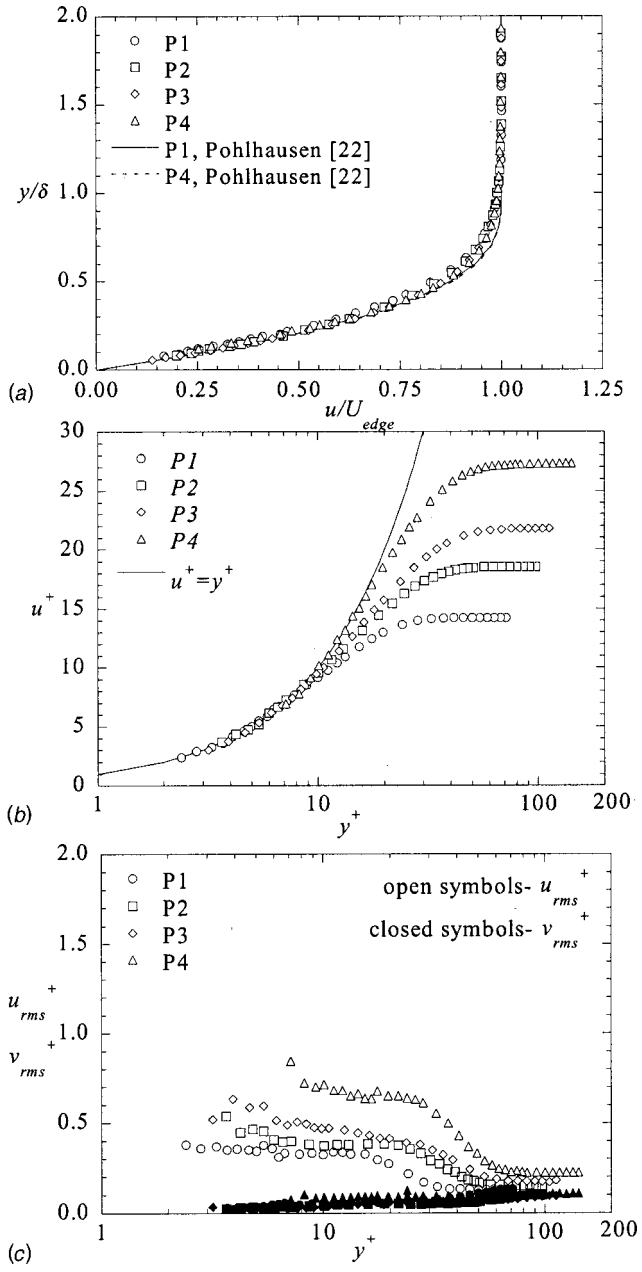

Fig. 8 Boundary layer profiles on the pressure surface at Tu = 0.6 percent plotted using: (*a*) freestream parameters, (*b*) inner wall scaling parameters, and (*c*) boundary layer profiles of streamwise (u^+_{rms}) and normal (v^+_{rms}) rms levels

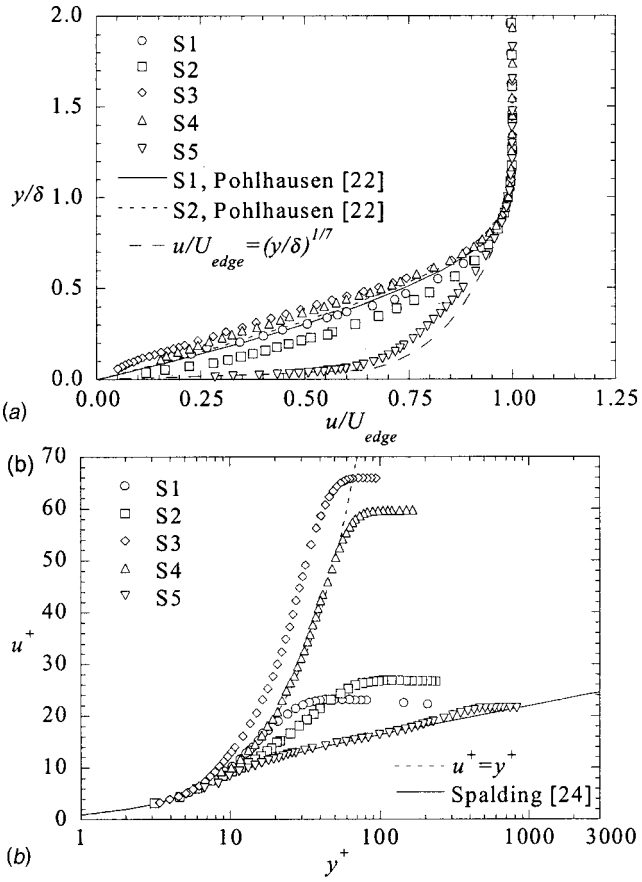

Fig. 9 Boundary layer profiles on the suction surface at Tu = 0.6 percent plotted using: (*a*) freestream parameters, and (*b*) inner wall scaling parameters

profile was generated using the WALZ program (Devenport et al. [23]). The Pohlhausen integral method is a function of the momentum thickness at each location. Only two profiles are displayed due to the similarity between the profiles on the pressure surface. As suggested by the agreement with the Pohlhausen [22] prediction, all four of the measured profiles on the pressure surface were laminar and collapsed onto a single curve when normalized by the boundary layer thickness and freestream velocity. The collapse of the mean velocity was a result of the constant favorable pressure gradient that caused similar boundary layer characteristics over the entire pressure surface. The linear portion of the profile, clearly indicated in Fig. 8(*a*) extended nearly 40 percent into the boundary layer from the wall for each of the profiles.

Figure 8(*b*) shows the mean velocity profiles plotted in terms of inner wall scaling parameters. Also presented in Fig. 8(*b*) is the linear relationship $u^+=y^+$. As can be seen, for the laminar profiles the measurement location nearest the wall typically corresponded to $y^+\sim 4$. Where the flow was linear in the near wall region, the use of inner wall scaling parameters collapsed the experimental data. As the flow progressed downstream, the decrease in the wall shear stress continually increased the u^+ values.

The streamwise ($u^+_{\rm rms}$) and normal ($v^+_{\rm rms}$) rms levels are given in Fig. 8(*c*). In general, the fluctuation levels are quite low with a maximum value of $u^+_{\rm rms}=0.9$ at the last streamwise location, $s/C=-0.6$. For a fully turbulent boundary layer at low freestream turbulence conditions the maximum streamwise rms levels reach a value of $u^+_{\rm rms}=2.8$ in the near wall region (Thole and Bogard [10]). The normal component is also given in Fig. 8(*c*) indicating essentially no fluctuations. As expected, the Reynolds shear stress profile, $\overline{u'v'}$, indicated no Reynolds shear stress was present in the boundary layers at low freestream turbulence conditions.

Suction Surface. Figure 9(*a*) shows the mean velocities measured on the suction surface using outer freestream scaling parameters. In addition to the measurements, a Pohlhausen [22] prediction for the boundary layers at an $s/C=0.21$ and $s/C=0.50$ are given along with a $1/7^{\rm th}$ law turbulent boundary layer approximation. The friction coefficient and Stanton number curves indicated the start of transition at location S2. For this reason the Pohlhausen [22] prediction, which is valid for laminar flows, is only given at locations S1 and S2. The measured boundary layer at location S1 agreed well with the laminar boundary layer prediction. The boundary layer at location S2 in the near wall region was fuller than the boundary layer at S1 and disagreed with the Pohl-

hausen prediction at location at S2. This should be expected because the friction coefficients showed the boundary layer was beginning to transition at this location. Just downstream of location S2 the adverse pressure gradient began, as shown in Fig. 4. At location S3, the adverse pressure gradient caused a decrease in the streamwise momentum near the wall. The decrease in momentum near the wall was still observed at location S4. The measured velocity profile at location S5 is similar to the $1/7^{th}$ power law approximation for a turbulent boundary layer. This indicates that the boundary layer was either near the end or just downstream of transition.

Figure 9(*b*) displays the measured mean velocity profiles on the suction surface in addition to the $u^+=y^+$ curve and Spalding's law (Spalding [24]). The first streamwise locations (S1) showed the typical laminar boundary layer behavior and agreement with the $u^+=y^+$ curve in the near wall region. The favorable acceleration gradient caused the boundary layer at location S2 to fall below the $u^+=y^+$ curve indicating a start of transition to a turbulent boundary layer. At location S3, the measured boundary layer was above the $u^+=y^+$ curve, which is again the result of the adverse pressure gradient. This result is consistent with the results from Mislevy and Wang [21] who also showed that laminar boundary layers were above the $u^+=y^+$ curve when subjected to an adverse pressure gradient. Farther downstream at location S4, the boundary has moved back towards the $u^+=y^+$ curve. At the farthest downstream location, S5, the boundary layer was turbulent with a depressed wake and showed good agreement with Spalding's law for a turbulent boundary layer.

The streamwise ($u^+_{\rm rms}$) and normal ($v^+_{\rm rms}$) rms levels are presented in Figs. 10(*a*) and 10(*b*). The first three streamwise locations (S1, S2, and S3) had a peak streamwise rms level of 1.5. Large fluctuations were observed at location S4. As discussed previously, for a fully turbulent boundary layer at low freestream turbulence conditions the maximum values of reach a value of $u^+_{\rm rms}=2.8$ in the near wall region (Thole and Bogard [10]). The values of $u^+_{\rm rms}=8$ that occurred at S4 were the result of the elevated turbulence existing in a boundary layer with low wall shear stress due to the adverse pressure gradient. The peak rms level at position S3 is higher by 20 percent relative to the S5 position, while the wall shear stress at position S3 is lower by 29 percent relative to the S5 position. Thereby, the two almost equally contribute to having high $u^+_{\rm rms}$ peaks. Similar behavior is noted by Lee and Kang [9] and Mislevy and Wang [25] in their results at their highest inlet turbulence level of 7 percent. Farther downstream at location S5, the magnitude of the streamwise rms levels reached a value of $u^+_{\rm rms}=3$ which was near the typical value for a fully turbulent boundary layer.

The normal rms levels (Fig. 10(*b*)) for the first three locations (S1, S2, and S3) indicated low levels throughout the boundary layer. At location S4 a large increase was observed with a peak level of $v^+_{\rm rms}=1.8$. Again, the higher values were the result of the elevated turbulence levels being present in a region of low wall shear stress. Downstream at location S5, an increase in the normal rms level was observed in the outer portion of the boundary layer. Inside the boundary layer, these levels flattened out and began to decrease as the result of attenuation of the vane surface. Thole and Bogard [9] showed that for a boundary layer at low freestream turbulence conditions, the normal rms levels should reach a maximum near $v^+_{\rm rms}=1$.

The Reynolds shear stress profiles ($\overline{u'v'}$) are given in Fig. 10(*c*). The first two locations where coincident LDV measurements were performed (S2 and S3) showed the absence of Reynolds shear stress. At location S4, near the start of transition, a peak in the Reynolds stress was observed away from the surface of the vane. The level of the turbulent shear stress has been shown by Mislevy and Wang [23] to increase dramatically in transitional boundary layers being subjected to an adverse pressure gradient. At this location, the turbulent shear stress was approximately 300 percent of the wall-generated shear stress. Proceeding farther downstream to location S5, the peak stress moved closer to the vane surface. At this location, the peak turbulent shear stress was approximately equal to the wall shear stress as is typically the case for a fully turbulent boundary layer.

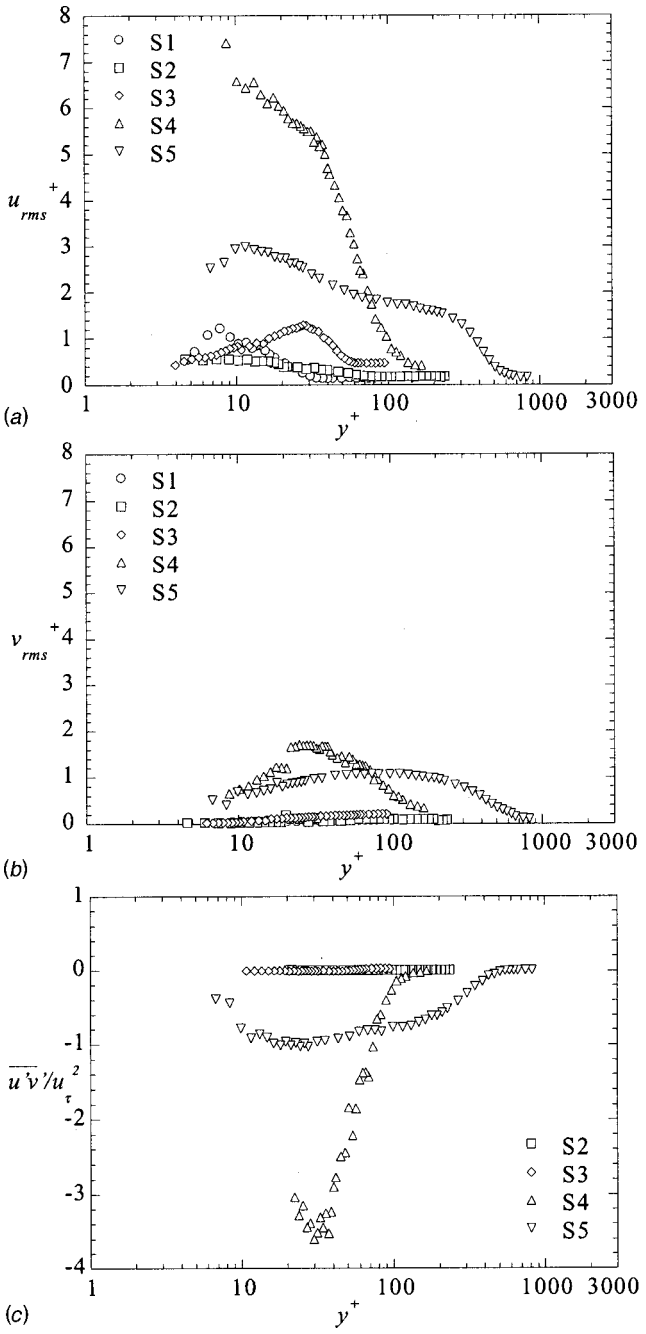

Fig. 10 Profiles of: (*a*) streamwise ($u^+_{\rm rms}$) (*b*) normal ($v^+_{\rm rms}$), and (*c*) Reynolds shear stress levels on the suction surface at Tu=0.6 percent plotted using inner wall scaling parameters

Boundary Layer at High Freestream Turbulence

Boundary layer measurements were performed at the same streamwise locations to allow for a direct determination of the effect of turbulence levels on boundary layer growth and development.

Pressure Surface. Figure 11(*a*) shows the mean velocity profiles measured on the pressure surface plotted in terms of

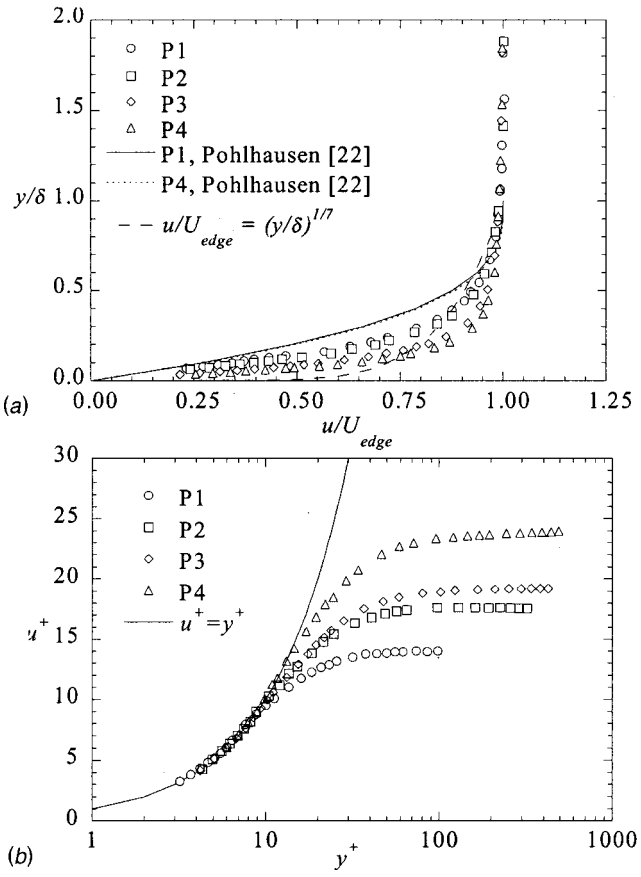

Fig. 11 Boundary layer profiles on the pressure surface at Tu=19.5 percent plotted using: (*a*) freestream parameters, and (*b*) inner wall scaling parameters

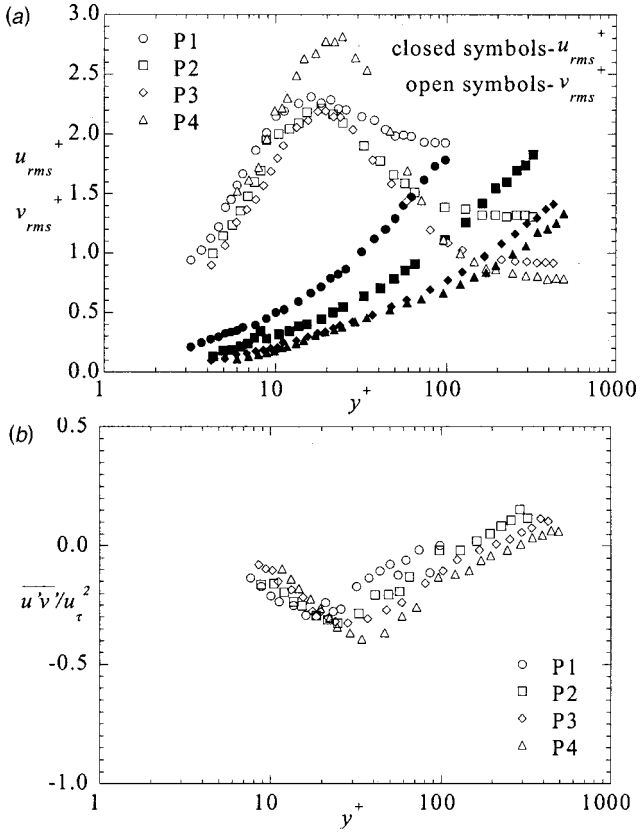

Fig. 12 Boundary layer profiles of: (*a*) streamwise (u_{rms}^+) and normal (v_{rms}^+) rms levels, and (*b*) Reynolds shear stress on the pressure surface at Tu=19.5 percent plotted using inner wall scaling parameters

freestream parameters at the 19.5-percent turbulence levels. Figure 11(*a*) also shows the Pohlhausen predictions at locations P1 and P4 as well as a $1/7^{th}$ turbulent profile. At low freestream turbulence conditions, shown previously in Fig. 8(*a*), all four of the measured profiles on the pressure surface were laminar and collapsed onto a single curve. At the high freestream turbulence conditions, the boundary layers did not agree with the Pohlhausen [21] predictions for a laminar boundary layer with no turbulence as shown by the discrepancy with the correlation given for the P1 and P4 locations. As expected from the increased shear stress, the velocity profiles in the near wall region were fuller than at low freestream turbulence levels. The first two streamwise locations (P1 and P2) showed a laminar velocity profile and still collapsed onto a single curve. At locations P3 and P4, where an increase in the friction coefficient was observed, the profiles had steeper velocity gradients in the near wall region.

Figure 11(*b*) presents the velocity profiles using inner wall scaling on the pressure side for the high freestream turbulence conditions. These boundary layer profiles are similar to the profiles displayed in Fig. 6(*b*) measured at 0.6 percent turbulence. The only noticeable difference between Fig. 8(*b*) and Fig. 11(*b*) was that the u^+ values level off to lower values for the 19.5-percent turbulence case as compared with the 0.6 percent turbulence case. This was the result of the high shear stress measured at the wall for the high freestream turbulence conditions as compared to the low freestream turbulence conditions.

The streamwise (u_{rms}^+) and normal (v_{rms}^+) rms levels are plotted using inner wall scaling parameters in Fig. 12(*a*). The streamwise rms levels increased from the values at the edge of the boundary layer to their maximum levels near a $y^+=20$. For a turbulent boundary layer, the maximum value of the streamwise rms levels were $u_{\mathrm{rms}}^+=2.8$ and occur at a location near $y^+=10$. For the first three streamwise positions (P1, P2, and P3) the maximum level in the boundary layer reached levels of $u_{\mathrm{rms}}^+=2.0$ at a location of $y^+\sim 20$. At location P4, the streamwise rms levels are higher reaching levels similar to those in a turbulent boundary layer. Moving closer to the wall, a sharp decrease in the streamwise rms levels was observed. Recall that the acceleration parameter was $K=3.4\times 10^{-6}$ along the pressure side of the airfoil. With such a large acceleration, one would expect that any boundary layer transition would be suppressed by the acceleration. The previously shown mean velocity profiles are in agreement with typical laminar profiles, but the large fluctuations indicate the presence of turbulence. The normal rms levels show a continual decrease in magnitude as the stator vane surface is approached as a result of being attenuated by the vane surface. It is interesting to note that the location of the peak fluctuating value is further away from the wall than that which would occur for a turbulent boundary layer profile along a flat plate. Figure 12(*a*) also indicates the anisotropy of the freestream turbulence outside the boundary layer, which is a result of the redistribution of the turbulence due to streamline curvature.

Normalized values of the Reynolds shear stress ($\overline{u'v'}/u_\tau^2$) are given in Fig. 12(*b*). For each of the cases the Reynolds stress was near zero at the edge of the boundary layer. At location P1 the Reynolds shear stress became negative in the boundary reaching a value of -0.3 at a $y^+=15$. Proceeding downstream the shear stress levels became increasingly negative reaching a value of $\overline{u'v'}/u_\tau^2=-0.4$ at a $y^+=30$ at location P4. The maximum Reynolds shear stress in the boundary layer was approximately 30 percent of the viscous shear stress measured at the wall for each of

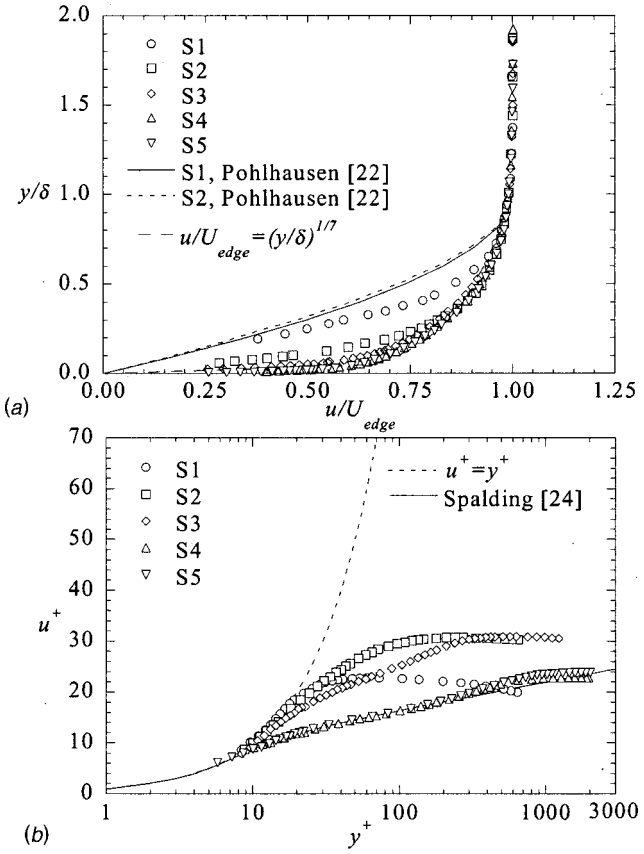

Fig. 13 Boundary layer profiles on the suction surface at Tu = 19.5 percent plotted using; (*a*) freestream parameters, and (*b*) inner wall scaling parameters

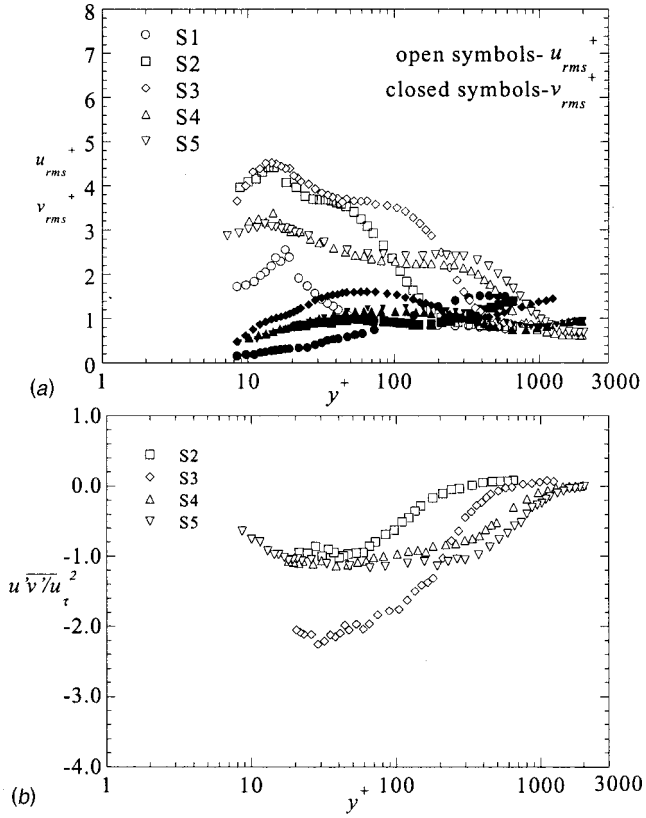

Fig. 14 Boundary layer profiles of: (*a*) streamwise (u^+_{rms}) and normal (v^+_{rms}) rms levels, and (*b*) Reynolds shear stress, on the suction surface at Tu = 19.5 percent plotted using inner scaling

the streamwise locations. Moving closer to the wall, the Reynolds shear stress approached zero for each of the streamwise locations. This was expected since the viscous shear dominates near the wall.

Suction Surface. The boundary layer profiles measured on the suction surface at 19.5-percent turbulence levels are plotted in Fig. 13(*a*) using boundary layer scaling parameters. The laminar profiles predicted by Pohlhausen [22] at locations S1 and S2 and the $1/7^{th}$ power law approximation for the turbulent boundary layer are also shown in Fig. 13(*a*). At location S1, the boundary layer was slightly fuller than the boundary layer measured at low freestream turbulence conditions. The measured boundary layers do not agree with the laminar profiles at S1 and S2 predicted by Pohlhausen [22] at high freestream turbulence levels. The profiles at S3 and S4 showed much fuller velocity profiles in the near wall region at higher turbulence than the low freestream turbulence conditions. This was the result of the earlier transition, which gave a higher momentum fluid in the boundary layer.

The streamwise velocity profiles on the suction surface are plotted using inner wall scaling parameters in Fig. 13(*b*). The boundary layer at location S1 was laminar, based upon the friction coefficients, and similar to the profiles measured at low freestream turbulence conditions shown in Fig. 10(*b*). The boundary layer started to transition from laminar to turbulent at locations S2 and S3. The transition at location S3 was obvious as shown by the deviation from the laminar profile for $50<y^+<200$. The boundary layers were fully turbulent at locations S4 and S5 and agreed well with Spalding's law. The strength of the wake, defined as the maximum deviation from the velocity distribution to the log-law in the outer region of the boundary layer, is larger at location S5 than S4. This is consistent with the higher momentum thickness Reynolds number at this location. The strength of the wake for these profiles was smaller than expected due to the presence of elevated turbulence in the freestream, but does indicate a negative wake strength. Negative wake strengths often occur for high freestream turbulence conditions (Thole and Bogard [10]).

The streamwise ($u^+_{\rm rms}$) and normal ($v^+_{\rm rms}$) rms levels are displayed using inner wall scaling parameters in Fig. 14(*a*). The $u^+_{\rm rms}$ levels at location S1, which was a laminar boundary layer, were high but lower than values for a fully turbulent boundary layer. At locations S2 and S3, the transitional boundary layer resulted in rms levels of $u^+_{\rm rms}=4$, which were higher than measured for a turbulent boundary layer. As discussed previously, this was due to the presence of the high turbulence levels in boundary layers with low wall shear stress. At locations S4 and S5, which were fully turbulent boundary layers, the maximum level in the boundary layers were $u^+_{\rm rms}=3$ which was only slightly higher than expected.

The normal rms ($v^+_{\rm rms}$) levels are also shown in Fig. 14(*a*). For the S1 location, the vrms+ levels showed a continuous decrease in magnitude through the boundary layer. At location S2, the levels in the boundary layer were higher than the levels for S1, indicating that the profile was on the onset of transition at this streamwise location. Farther downstream at S3, the normal fluctuations reached a maximum of $v^+_{\rm rms}=1.5$. These values are larger than the typical value of $v^+_{\rm rms}=1$ for a turbulent boundary layer, and were the result of the fluctuations being present in the boundary layer. The values at S4 and S5 agreed with the expected values for a turbulent boundary layer.

The Reynolds shear stress profiles are shown in Fig. 14(*b*). The boundary layer at location S2 contained Reynolds shear stress

indicating that it was at the onset of transition. At location S3, the maximum Reynolds shear stress in the boundary layer was approximately twice the measured viscous shear stress at the wall. For the fully turbulent boundary layers at locations S4 and S5, the maximum Reynolds stress in the boundary layer was approximately equal to the viscous shear stress deduced from the velocity gradient.

Conclusions

Detailed boundary layer measurements on a turbine vane geometry at combustor turbulence levels have been compared to boundary layer measurements at low turbulence levels. To date, this data has not been available in the literature and was made possible by using a large-scale test facility.

The integral boundary layer parameters at low freestream turbulence levels agreed well with those estimated using Thwaites' method when the boundary layer remained laminar. At high freestream turbulence levels, the integral parameters on the suction side indicated the transition location moved upstream of the transition location that had occurred at low freestream turbulence conditions. This upstream shift was also seen in the skin friction and heat transfer measurements. Overall lower shape factors occurred for the high freestream turbulence case as compared with the low freestream turbulence case indicating lower displacement to momentum thickness ratios. This is expected since lower shape parameters occur for turbulent boundary layers compared to laminar boundary layers.

At low freestream turbulence levels, the mean velocity profiles along the pressure side of the vane collapsed to a single curve using the edge velocity and boundary layer thicknesses as the scaling parameter. The profiles also indicated a linear behavior of velocity with distance from the wall in the near-wall region, even though the boundary layer is affected by a pressure gradient. At high turbulence levels, the outer scaling parameters did not collapse the profiles. At high freestream turbulence levels, fluctuations were measured in the boundary layer along the pressure side even though the mean profiles were more consistent with a laminar-like boundary layer. At the most downstream positions measured along the suction side, the mean velocity profiles indicated a fully turbulent profile with a depressed wake region.

The data presented in this paper provide the community with an understanding of the effects that high freestream turbulence can have on the development of an airfoil boundary layer. In addition, this data provides not only surface phenomena but also velocity field measurements to use for improving predictive turbulence models.

Appendix A1

Boundary Layer Parameters at Low Turbulence Conditions

Pressure Surface	U_{edge} (m/s)	Tu	$C_f/2$	δ/C	δ^*/C	θ/C	H
P1	4.99	0.8%	0.0049	0.0025	7.09E−4	3.01E−4	2.35
P2	8.69	0.8%	0.0029	0.0026	7.24E−4	3.17E−4	2.29
P3	13.11	0.6%	0.0021	0.0026	6.91E−4	3.04E−4	2.27
P4	18.65	0.7%	0.0013	0.0024	6.76E−4	2.80E−4	2.42
Suction Surface			$C_f/2$	δ/C	δ^*/C	θ/C	H
S1	23.54	0.5%	0.0019	0.0010	3.49E−4	1.33E−4	2.63
S2	31.23	0.6%	0.0014	0.0020	5.51E−4	2.58E−4	2.14
S3	30.04	0.6%	0.0002	0.0033	1.40E−4	4.58E−4	3.05
S4	28.97	2.1%	0.0003	0.0044	1.71E−4	6.08E−4	2.81
S5	27.56	2.2%	0.0022	0.0097	1.56E−4	1.08E−3	1.44

Appendix A2

Boundary Layer Parameters at High Turbulence Conditions

Pressure Surface	U_{edge} (m/s)	Tu	$C_f/2$	δ/C	δ^*/C	θ/C	H
P1	5.43	12.1%	0.0051	0.0034	6.80E−4	3.22E−4	2.11
P2	9.22	7.1%	0.0032	0.0037	6.79E−4	3.29E−4	2.06
P3	13.43	4.9%	0.0027	0.0046	6.55E−4	3.57E−4	1.83
P4	18.96	3.7%	0.0018	0.0055	6.89E−4	3.78E−4	1.82
Suction Surface			$C_f/2$	δ/C	δ^*/C	θ/C	H
S1	23.31	3.9%	0.0019	0.0012	3.41E−4	1.30E−4	2.62
S2	31.02	4.0%	0.0011	0.0040	7.25E−4	3.78E−4	1.92
S3	30.05	3.6%	0.0011	0.0097	1.52E−3	9.78E−4	1.56
S4	28.99	3.4%	0.0019	0.0180	2.41E−3	1.74E−3	1.38
S5	27.61	3.7%	0.0018	0.0259	3.34E−3	2.44E−3	1.36

Acknowledgments

The authors would like to acknowledge the Department of Energy-Advanced Gas Turbine Systems Research Program for their support. Partial support for this work also came from Pratt & Whitney.

Nomenclature

C = true chord of stator vane
$C_j(C_{fo})$ = friction coefficient (low turbulence case), $2(u_\tau^2/U_{edge}^2)$
C_p = specific heat
d = turbulence generator rod diameter
D^+ = probe volume diameter in inner coordinates, Du_τ/ν
h = convective heat transfer coefficient
H = shape factor, δ^*/θ
L_ε = dissipation length scale, $1.5u_{rms}^2/\varepsilon$
K = acceleration parameter, $\nu(dU_{edge}/ds)/U_{edge}^2$
P = vane pitch
Pr = Prandtl number
Re = Reynolds number defined as $Re=sU_{edge}/\nu$
Re_{in} = Reynolds number defined as $Re=CU_{in}/\nu$
s = surface distance along vane measured from stagnation
s_L = turbulence generator bar spacing
S = span of vane
$St(St_o)$ = Stanton number (low turbulence case) $St=h/\rho CpU_{edge}$
Tu = turbulence level $(0.5(u_{rms}{}^2+v_{rms}{}^2))^{0.5}/U_{edge}$
u_τ = shear velocity, $\sqrt{\tau_w/\rho}$
u^+ = velocity in inner coordinates, u/u_τ
u, v, w = mean local velocity in local coordinate system
U_{inlet} = incident upstream velocity
U_{edge} = local inviscid velocity
$U, \underline{V, W}$ = mean velocity in the X, Y, Z directions
$\overline{u'v'}$ = Reynolds shear stress
x, y, z = local coordinates defined at measurement location
X, Y, Z = global coordinates defined from stagnation location
y^+ = velocity in inner coordinates, yu_τ/ν
δ = boundary layer thickness
δ^* = displacement thickness
ε = turbulent dissipation rate
θ = momentum thickness
Λ_x = integral length scale

ρ = density
τ_w = wall shear stress
ν = viscosity

Subscripts

edge = local inviscid quantity
inlet = inlet
rms = root mean square

References

[1] Goldstein, R. J., Lau, K. Y., and Leung, C. C., 1983, ''Velocity and Turbulence Measurements in Combustion Systems,'' Exp. Fluids, **1**, pp. 93–99.
[2] Kuotmos, P., and McGuirk, J. J., 1989, ''Isothermal Flow in a Gas Turbine Combustor—A Benchmark Experimental Study,'' Exp. Fluids, **7**, pp. 344–354.
[3] Goebel, S. G., Abuaf, N., Lovett, J. A., and Lee, C. P., 1993, ''Measurements of Combustor Velocity and Turbulence Profiles,'' ASME Paper No. 93-GT-228.
[4] Moss, R. W., 1992, ''The Effects of Turbulence Length Scale on Heat Transfer,'' University of Oxford, Department of Engineering Science, Report No. OUEL 1924, Ph.D. dissertation.
[5] Radomsky, R., and Thole, K. A., 2000, ''Highly Turbulent Flowfield Measurements Around a Stator Vane,'' ASME J. Turbomach., **122**, pp. 255–262.
[6] Kestin, J., 1966, ''The Effect of Freestream Turbulence on Heat Transfer Rates,'' Advances in Heat Transfer, 3, New York, Academic Press.
[7] Ubaldi, M., Zunino, P., Campora, U., and Ghiglione, A., 1996, ''Detailed Velocity and Turbulence Measurements of the Profile Boundary Layer in a Large Scale Turbine Cascade,'' ASME Paper No. 96-GT-42.
[8] Bario, F., and Beral, C., 1998, ''Boundary Layer Measurements on the Pressure and Suction Sides of a Turbine Inlet Guide Vane,'' Exp. Therm. Fluid Sci., **17**, pp. 1–9.
[9] Lee, H., and Kang, S.-H., 2000, ''Flow Characteristics of Transitional Boundary Layers on an Airfoil in Wakes,'' ASME J. Fluids Eng., **122**, pp. 522–532.
[10] Thole, K. A., and Bogard, D. G., 1996, ''High Freestream Turbulence Effects on Turbulent Boundary Layers,'' ASME J. Fluids Eng., **118**, No. 2, pp. 276–284.
[11] Radomsky, R., and Thole, K. A., 2000, ''High Freestream Turbulence Effects in the Endwall Leading Edge Region,'' ASME J. Turbomach., **122**, pp. 699–708.
[12] Kang, M., Kohli, A., and Thole, K. A., 1999, ''Heat Transfer And Flowfield Measurements In The Leading Edge Region of a Stator Vane Endwall,'' ASME J. Turbomach., **121**, pp. 558–568.
[13] Kang, M., and Thole, K. A., 2000, ''Flowfield Measurements in the Endwall Region of a Stator Vane,'' ASME J. Turbomach., **122**, pp. 458–466.
[14] Radomsky, R., and Thole, K. A., 2000, ''Measurements and Predictions of a Highly Turbulent Flowfield in a Turbine Vane Passage,'' ASME J. Fluids Eng., **122**, pp. 666–676.
[15] Polanka, M., 1999, ''Detailed Film Cooling Effectiveness and Three Component Velocity Field Measurements on a First Stage Turbine Vane Subject to High Freestream Turbulence,'' Ph.D. dissertation, University of Texas-Austin.
[16] Radomsky, R. W., 2000, ''High Freestream Turbulence Studies on a Scaled-up Stator Vane,'' University of Wisconsin, Department of Mechanical Engineering, Ph.D. dissertation.
[17] Kays, W. M., and Crawford, M. E., 1991, *Convective Heat and Mass Transfer*, McGraw-Hill, New York, NY.
[18] Moffat, R. J., 1988, ''Describing the Uncertainties in Experimental Results,'' Exp. Therm. Fluid Sci., **1**, pp. 3–17.
[19] Thwaites, B., 1949, ''Approximate Calculation of the Laminar Boundary Layer,'' Aeronaut. Q., **1**, pp. 245–280.
[20] Schetz, J. A., 1993, *Boundary Layer Analysis*, Prentice-Hall, New York.
[21] Mislevy, S. P., and Wang, T., 1996, ''The Effects of Adverse Pressure Gradients on Momentum and Thermal Structures in Transitional Boundary Layers: Part 1-Mean Quantities,'' ASME J. Turbomach., **118**, pp. 717–727.
[22] Pohlhausen, K., 1921, ''On the Approximate Integration of the Differential Equations of Laminar Shear Layers,'' Z. Angew. Math. Mech., **1**, pp. 252–268.
[23] Devenport, W. J., Kapania, R., Rojiani, K., and Singh, K., ''Java Applets for Engineering Education,'' http://www.engapplets.vt.edu (Virginia Tech, 2000).
[24] Spalding, D. B., 1961, ASME J. Appl. Mech., **28**, pp. 455–457.
[25] Mislevy, S. P., and Wang, T., 1996b, ''The Effects of Adverse Pressure Gradients on Momentum and Thermal Structures in Transitional Boundary Layers: Part 2-Fluctuation Quantities,'' ASME J. Turbomach., **118**, pp. 728–736.